

**FULL PAPER**Applied
Organometallic
Chemistry

WILEY

Pd nanoparticles supported on reduced graphene oxide as an effective and reusable heterogeneous catalyst for the Mizoroki–Heck coupling reaction

Maryam Mirza-Aghayan¹ | Marzieh Mohammadi¹ | Ahmed Addad² | Rabah Boukherroub³

¹Chemistry and Chemical Engineering Research Center of Iran, PO Box 14335-186, Tehran, Iran

²University of Lille, CNRS, UMR 8207 – UMET, F-59000, Lille, France

³University of Lille, CNRS, Centrale Lille, ISEN, Univ. Valenciennes, UMR 8520 - IEMN, F-59000, Lille, France

Correspondence

Maryam Mirza-Aghayan, Chemistry and Chemical Engineering Research Center of Iran, PO Box 14335-186. Tehran, Iran.
Email: m.mirzaaghayan@ccerci.ac.ir

A general method for the synthesis of palladium nanoparticles loaded on reduced graphene oxide functionalized with diethylenetriamine (PdNPs/rGO-NH₂) using a sonochemical procedure is described. The heterogeneous nanocomposite was characterized by Fourier transform infrared spectroscopy, X-ray diffraction, scanning electron microscopy, energy dispersive X-ray, thermogravimetric analysis, high-angle annular dark field scanning transmission electron microscopy, X-ray photoelectron spectroscopy, UV-visible absorption, and inductively coupled plasma optical emission spectrometry. The PdNPs/rGO-NH₂ was very effective for the Mizoroki–Heck coupling reaction of several aryl iodide compounds with different alkenes in the presence of triethylamine. The reaction provides the coupling products in good to excellent yields (59–100%). Additionally, the PdNPs/rGO-NH₂ catalyst can be reutilized for six successive runs without any apparent diminution of its catalytic reactivity.

KEY WORDS

diethylenetriamine, Mizoroki–Heck coupling reaction, palladium nanoparticles, reduced graphene oxide

1 | INTRODUCTION

C–C bond formation is of essential importance in organic synthesis^[1–3] and several methods are described in the literature for this chemical process. Most of the useful procedures for C–C bond formation involve Grignard,^[4] aldol,^[5] Michael,^[6] alkylation,^[7] and cross-coupling reactions mediated by metal catalysts, such as the Suzuki–Miyaura,^[8] Sonogashira,^[9] and Mizoroki–Heck^[10] reactions. Several metallic catalysts have been extensively considered for cross-coupling reactions, but the use of palladium catalysts has generated great attention because of their remarkable performance for this reaction. Several homogenous and heterogeneous palladium catalysts,^[11] such as Pd⁺² complex with *ter*-bis(diphenylphosphinomethyl)amino ligands,^[12] and

Schiff base-derived Pd catalysts^[11a] as homogenous catalysts, mobil composition of matter-48 (MCM-48) supported 2-pyridinylmethanimine Pd catalyst,^[13] supported ionic liquid phase Pd (SILP-Pd) catalysts,^[14] and Pd nanoparticles loaded onto graphene derivatives^[15] like heterogeneous catalysts have been investigated for cross-coupling reactions. However, homogeneous Pd catalysts face many difficulties, such as toxicity and low stability, difficulty in recovering, and a catalytic activity loss due to their precipitation and aggregation in the form of metallic palladium.^[16] To overcome these serious hurdles, heterogeneous catalysts have been successfully employed in recent years.^[13–15]

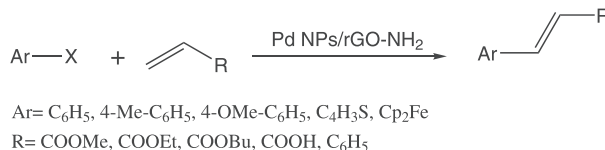
Graphite oxide and graphene derivatives have been successfully applied as efficient heterogeneous materials for various chemical transformations.^[17–22] For instance,

Pd nanoparticles (PdNPs) loaded on graphene turned out to be an effective catalyst in the Suzuki–Miyaura coupling reaction.^[15] Recently, we have investigated the use of the palladium nanoparticles loaded on reduced graphene oxide (PdNPs/rGO) nanocomposite in the presence of triethylsilane for the reduction of alcohol compounds to their respective methylene derivatives.^[23] In continuation of our investigation of graphite oxide^[19–22] and its derivatives,^[23] we report a general method for the preparation of PdNPs loaded on reduced graphene oxide functionalized with diethylenetriamine (PdNPs/rGO-NH₂). The PdNPs/rGO-NH₂ material was identified by different analytical tools and its catalytic activity was examined for C–C bond formation via the Mizoroki–Heck coupling reaction (Schemes 1 and 2).

2 | EXPERIMENTAL

2.1 | Preparation of rGO-NH₂

A mixture of diethylenetriamine (500 mg, 5 mmol) and GO (50 mg) in 50 ml of ethanol was sonicated using an Elmasonic P ultrasonic cleaning unit for 3 hr at ambient

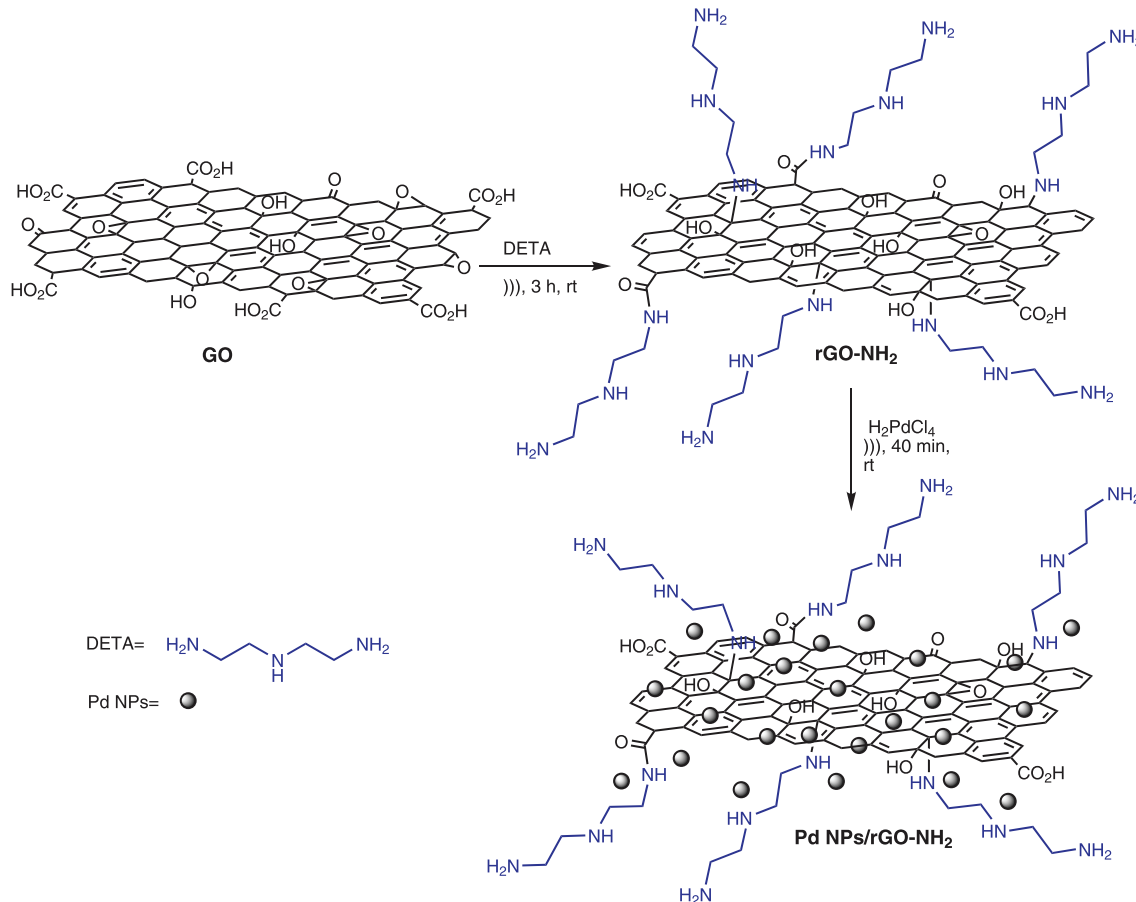


SCHEME 2 Mizoroki–Heck coupling reaction

temperature. The resulting solution was centrifuged and washed sequentially with ethanol, methanol, and acetone. The rGO-NH₂ was obtained by dehydration at room temperature overnight.

2.2 | Preparation of PdNPs/rGO-NH₂ material

A suspension of 200 mg of rGO-NH₂ in 200 ml of deionized H₂O was dispersed by an ultrasonic cleaning unit for 120 min at room temperature. Then 10 ml of GO dispersion in 100 ml of deionized H₂O was mixed for 20 min using an ultrasonic cleaning unit. Next, 4 ml of H₂PdCl₄ solution, obtained by fully dissolving PdCl₂ (177 mg) in 100 ml of 20 mM HCl solution, was introduced into this mixture and sonicated for 40 min by an



SCHEME 1 Preparation of heterogeneous PdNPs loaded onto rGO functionalized with diethylenetriamine nanocomposite

ultrasonic homogenizer. PdNPs/rGO-NH₂ was obtained by centrifugation, washed with deionized H₂O, filtered, and dehydrated in an oven at 80°C for 120 min.

2.3 | General method for the Mizoroki-Heck reaction

PdNPs/rGO-NH₂ nanocomposite (4 mg, 6.4 × 10⁻³ mmol) was added to a solution of aromatic iodide compound (0.5 mmol), alkene (1 mmol), and triethylamine (Et₃N) (2 mmol) in dimethylformamide (DMF) (2 ml) as solvent. The resulting solution was reacted at 120°C for 4 hr prior to gas chromatographic analysis. For catalyst separation, the mixture was centrifuged and washed with ethanol and then dried under vacuum for reuse. The organic solution was extracted with ethyl acetate (3 × 20 ml) and dried over MgSO₄. The solvent was evaporated and the crude mixture was isolated by column chromatography with hexane/ethyl acetate (8/1). The known products were identified by ¹H NMR and the unknown products were fully identified by ¹H and ¹³C NMR, mass spectroscopy and Fourier transform infrared (FT-IR) spectroscopy. All data are presented in the Supporting Information Data S1 file.

Methyl (*E*)-3-(ferrocenyl)acrylate (entry 5, Table 2); ¹H NMR (500 MHz, CDCl₃): δ = 3.78 (s, 3H, OCH₃), 4.17 (s, 5H, (C₅H₅)), 4.42 (m, 2H, C₅H₄), 4.50 (m, 2H, C₅H₄), 6.05 (d, *J* = 15.7 Hz, 1H, CH), 7.59 (d, *J* = 15.7 Hz, 1H, CH); ¹³C NMR (125 MHz, CDCl₃): δ = 51.74, 68.89, 69.92, 70.92, 114.69, 146.20, 150.77, 167.53; MS (EI) (70 eV), *m/z* (%): 270 (100) [M]⁺, 239 (6) [M-OCH₃]⁺, 205 (63), 175 (32), 147 (7), 121 (25), 89 (12), 56 (14); IR (KBr): ν = 2946, 1713, 1630, 1435, 1352, 1307, 1193, 1158, 1030, 975, 805, 475 cm⁻¹.

(*E*)-3-(Ferrocenyl)acrylate (entry 7, Table 2); ¹H NMR (500 MHz, CDCl₃): δ = 1.36 (t, *J* = 7.1 Hz, 3H, CH₃), 4.17 (s, 5H, (C₅H₅)), 4.24 (q, *J* = 7.1 Hz, 2H, OCH₂), 4.42 (m, 2H, C₅H₄), 4.50 (m, 2H, C₅H₄), 6.04 (d, *J* = 15.7 Hz, 1H, CH), 7.58 (d, *J* = 15.7 Hz, 1H, CH); ¹³C NMR (125 MHz, CDCl₃): δ = 167.55, 145.87, 115.79, 70.95, 69.98, 68.54, 60.14, 14.33; MS (EI) (70 eV), *m/z* (%): 284 (100) [M]⁺, 256 (32) [M-1-C₂H₅]⁺, 239 (9) [M-OC₂H₅]⁺, 219 (23), 207 (35), 191 (23), 175 (24), 145 (11), 121 (26), 89 (17), 56 (15); IR (KBr): ν = 2918, 2850, 1703, 1636, 1464, 1366, 1314, 1205, 1037, 812, 479 cm⁻¹.

3 | RESULTS AND DISCUSSION

3.1 | Characterization of the PdNPs/rGO-NH₂ material

Ultrasonic irradiation was successfully applied for the synthesis of PdNPs/rGO-NH₂ nanocomposite. It should

be noted that ultrasound can generate a cavitation bubble where the reactants that entered during its formation are subjected to extreme conditions of temperature and pressure on collapse, leading to chemical reaction between them. This cavitation bubble collapse provides the energy needed for a chemical reaction. As shown in Scheme 1, rGO-NH₂ was synthesized from the direct reaction of GO with diethylenetriamine using ultrasonic irradiation. The mechanical effect of ultrasound provides the energy needed for this chemical reaction. By addition of H₂PdCl₄ to rGO-NH₂, the heterogeneous PdNPs/rGO-NH₂ nanocomposite was effectively formed. The PdNPs/rGO-NH₂ material was fully identified by FT-IR, X-ray diffraction (XRD), scanning electron microscopy (SEM), energy dispersive X-ray (EDX), thermogravimetric analysis (TGA), high-angle annular dark field scanning transmission electron microscopy (HAADF-STEM), X-ray photoelectron spectroscopy (XPS), transmission electron spectroscopy (TEM), UV-visible absorption, and inductively coupled plasma optical emission spectrometry (ICP-OES).

The FT-IR spectra of the starting GO, rGO-NH₂, and PdNPs/rGO-NH₂ nanocomposite are depicted in Figure 1. The FT-IR spectrum of GO displays characteristic stretching vibrations at 1726 cm⁻¹ (C=O in carbonyl and carboxylic acid groups), 1622 cm⁻¹ (C=C in an aromatic ring), 1380 cm⁻¹ (C-OH), 1200 cm⁻¹, and 1045 cm⁻¹ (C-O in epoxy and alkoxy groups, respectively) (Figure 1a).^[24] The spectrum of rGO-NH₂ reveals broad peaks at about 2918, 2863, and 1453 cm⁻¹ ascribed to the stretching vibrations of the CH₂ groups in diethylenetriamine. The presence of new peaks at 1112 and 1063 cm⁻¹ (C-N stretching vibrations) in the FT-IR spectrum of rGO-NH₂ indicates amide and/or amine bond formation (Figure 1b).^[25] A significant decrease in the peaks at 1726 and 1200 cm⁻¹ was observed, suggesting partial elimination of the oxygen groups and restoration of the graphenic structure. This is corroborated by the presence of a band at 1636 cm⁻¹ that can be attributed to C=C stretching vibrations in aromatic ring, indicating incomplete restoration of the graphene network in this procedure (Figure 1b). The FT-IR spectrum of the PdNPs/rGO-NH₂ material depicts typical bands at 3408, 1620, 1404, and 1040 cm⁻¹ ascribed to the stretching vibrations of OH, C=C, NH, and C-O groups, respectively (Figure 1c). It should be noted that the bonding between Pd and rGO can take place through hydrogen bonding or van der Waals forces with the -OH, -COOH, -NH, and C=O groups on the functionalized rGO-NH₂.^[26,27]

Figure 2 displays the XRD patterns of rGO-NH₂ and PdNPs/rGO-NH₂ nanocomposite. The XRD pattern of GO exhibits a distinct and characteristic peak at

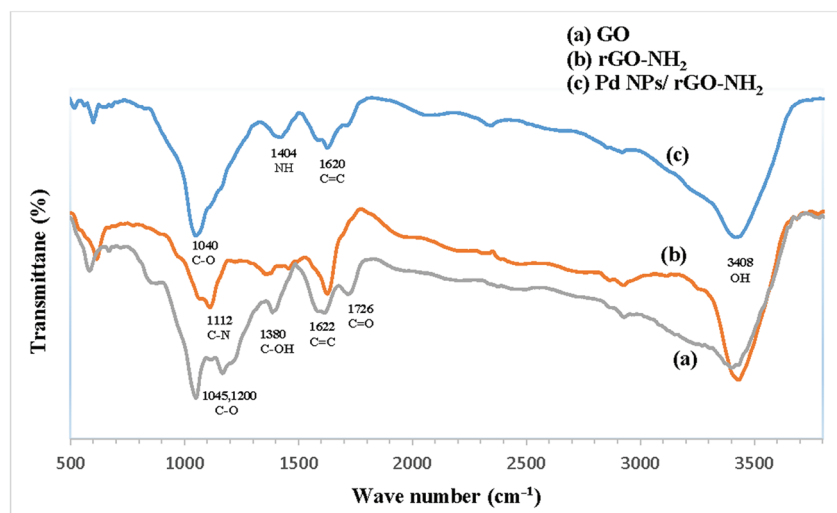


FIGURE 1 FT-IR transmission spectra of (a) GO, (b) rGO-NH₂, and (c) Pd NPs/rGO-NH₂ nanocomposite

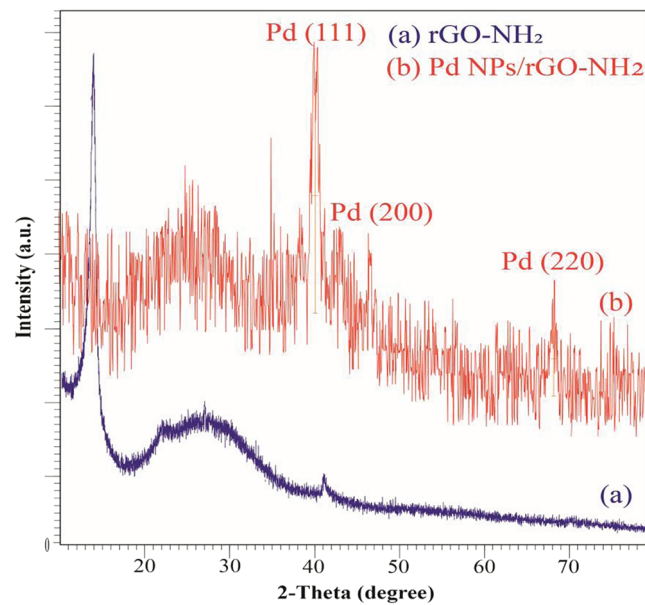


FIGURE 2 XRD patterns of (a) rGO-NH₂ and (b) PdNPs/rGO-NH₂ nanocomposite

$2\theta = 11.8^\circ$ (data not shown).^[28] The XRD pattern of rGO-NH₂ depicts a characteristic peak at $2\theta = 11.8^\circ$ for GO and a wide peak at about $2\theta = 26^\circ$ due to the presence of reduced graphene oxide (rGO) by elimination of oxygenated functional groups^[29,30] (Figure 2a). The XRD of PdNPs/rGO-NH₂ consists of peaks at $2\theta = 40.01^\circ$, 46.54° , and 67.93° attributed, respectively, to the (111), (200), and (220) crystalline planes of Pd (Figure 2b), confirming the presence of Pd⁰ in the nanocomposite.^[29,30] It also includes a wide peak at $2\theta = 26^\circ$, indicating the existence of rGO by elimination of oxygenated functional groups.^[31]

Figure 3 depicts SEM images along with EDX analysis. The comparison of the EDX analyses of GO and rGO-NH₂ reveals that chemical changes have occurred during

the reaction of GO with diethylenetriamine using ultrasonic irradiation (Figure 3d–f). The EDX spectrum of rGO-NH₂ clearly shows the presence of nitrogen (11.72 at%), which indicates the grafting of amino groups on the rGO sheet using this procedure (Figure 3e). EDX examination of the PdNPs/rGO-NH₂ material reveals the presence of Pd (Figure 3f). The palladium loading on PdNPs/rGO-NH₂ nanocomposite is estimated to be 25.46 wt% by EDX analysis (Figure 3f). This value is slightly higher than the 17.86 wt% (1.60 mmol/g) determined by ICP-OES analysis.

Figure 4 shows the thermogravimetric analysis (TGA) curves of GO and rGO-NH₂ materials. The weight loss of GO takes place in three consecutive steps: a weight loss of ~6% at around 106°C (desorption of H₂O molecules), 30% at $106\text{--}210^\circ\text{C}$ (decomposition of organic functional groups), and 22% in the temperature range of $210\text{--}900^\circ\text{C}$ due to the decomposition of the carbon skeleton (Figure 4a).^[23] The weight loss of rGO-NH₂ material, which is very similar to GO, also comprises three consecutive steps: a weight loss of ~6% at $\sim 106^\circ\text{C}$ which can be attributed to the dehydration of adsorbed H₂O molecules, a second weight loss of 22% ($106\text{--}210^\circ\text{C}$) due to the decomposition of the labile functional groups such as epoxy, OH, C=O, COOH, and NH, and a final step of a weight loss of 21% ($210\text{--}900^\circ\text{C}$), which can be attributed to the combustion of the carbon frame (Figure 4b).

HAADF-STEM images of PdNPs/rGO-NH₂ are depicted in Figure 5. High-angle annular dark field scanning transmission electron microscopy (HAADF-STEM) and high-angle annular dark field scanning transmission electron microscopy and energy dispersive X-ray (HAADF-STEM-EDX) elemental mapping were investigated to explore the elemental distribution of PdNPs/rGO-NH₂ nanocomposite. The results showed five dominant elements (Pd, C, O, Cl, and N) present in the

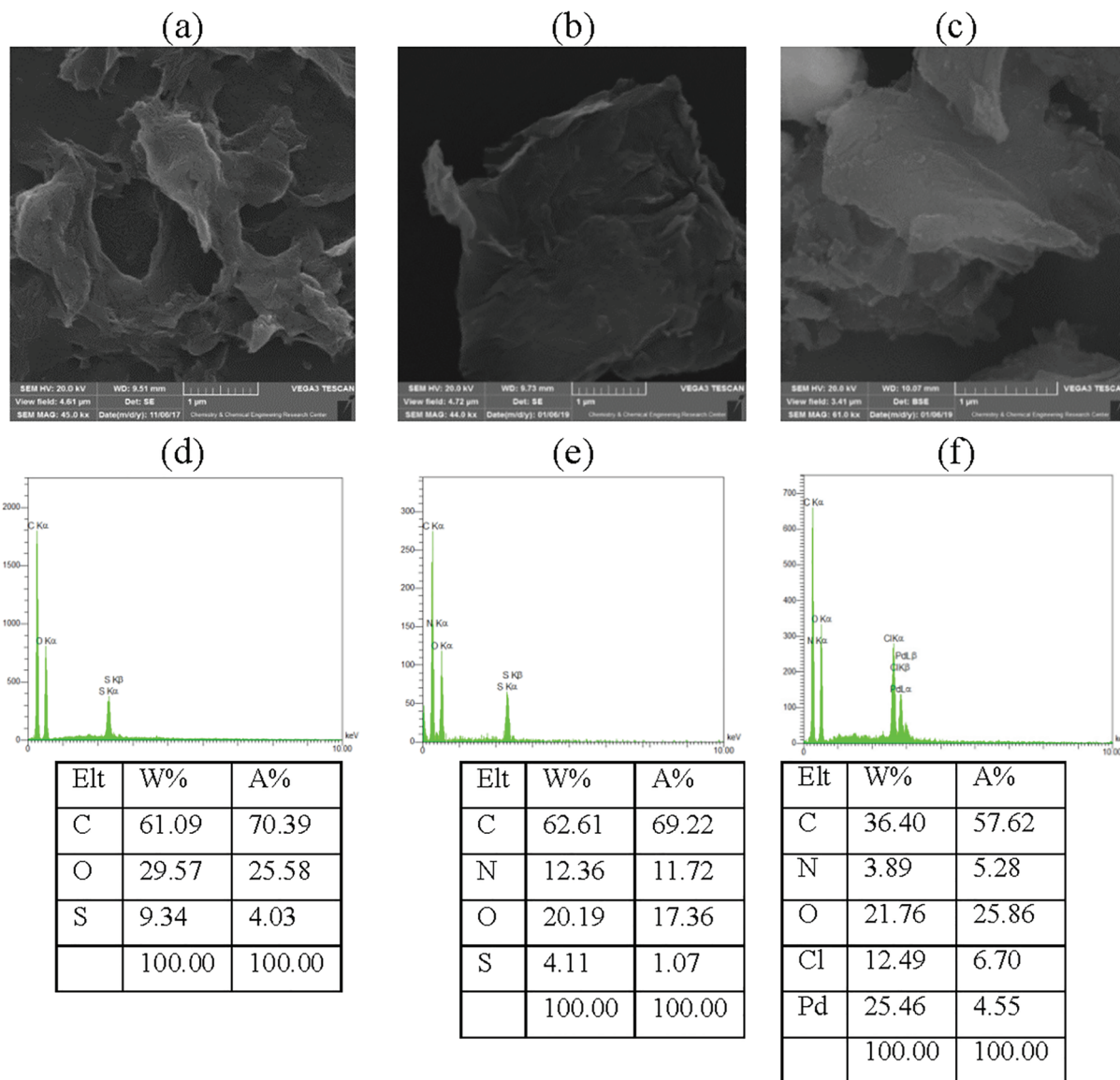


FIGURE 3 The SEM images of (a) GO, (b) rGO-NH₂, and (c) PdNPs/rGO-NH₂ material, and (d)–(f) their relevant EDX spectra

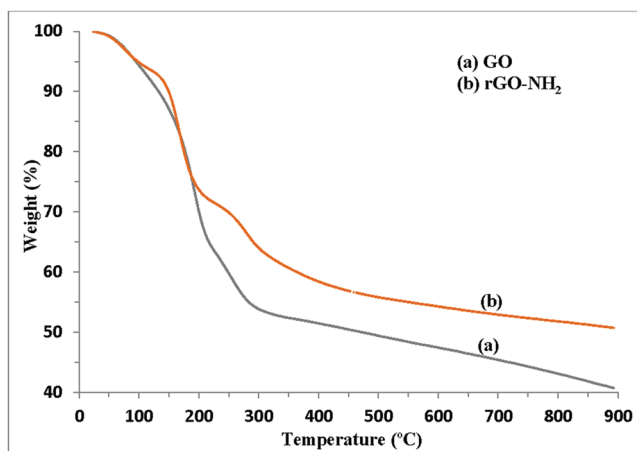


FIGURE 4 TGA analysis of (a) GO and (b) rGO-NH₂ material

PdNPs/rGO-NH₂ material. The presence of N and Pd indicates that diethylenetriamine and palladium are homogeneously distributed on the rGO surface, in complete agreement with EDX analysis.

TEM imaging of the synthesized PdNPs/rGO-NH₂ revealed exfoliated rGO sheets which are coated homogeneously with PdNPs of 2.1 nm average size (Figure 6). By focusing on the nanocomposite, crystallized PdNPs were observed. Additionally, high resolution transmission electron microscopy (HRTEM) analysis of a single Pd nanoparticle revealed lattice fringes with a d-spacing of 0.23 nm, which correspond to the {111} lattice planes of the face-centered cubic (fcc) structure of Pd.

The elemental composition of rGO-NH₂ nanocomposite was identified by XPS (Figure 7). The

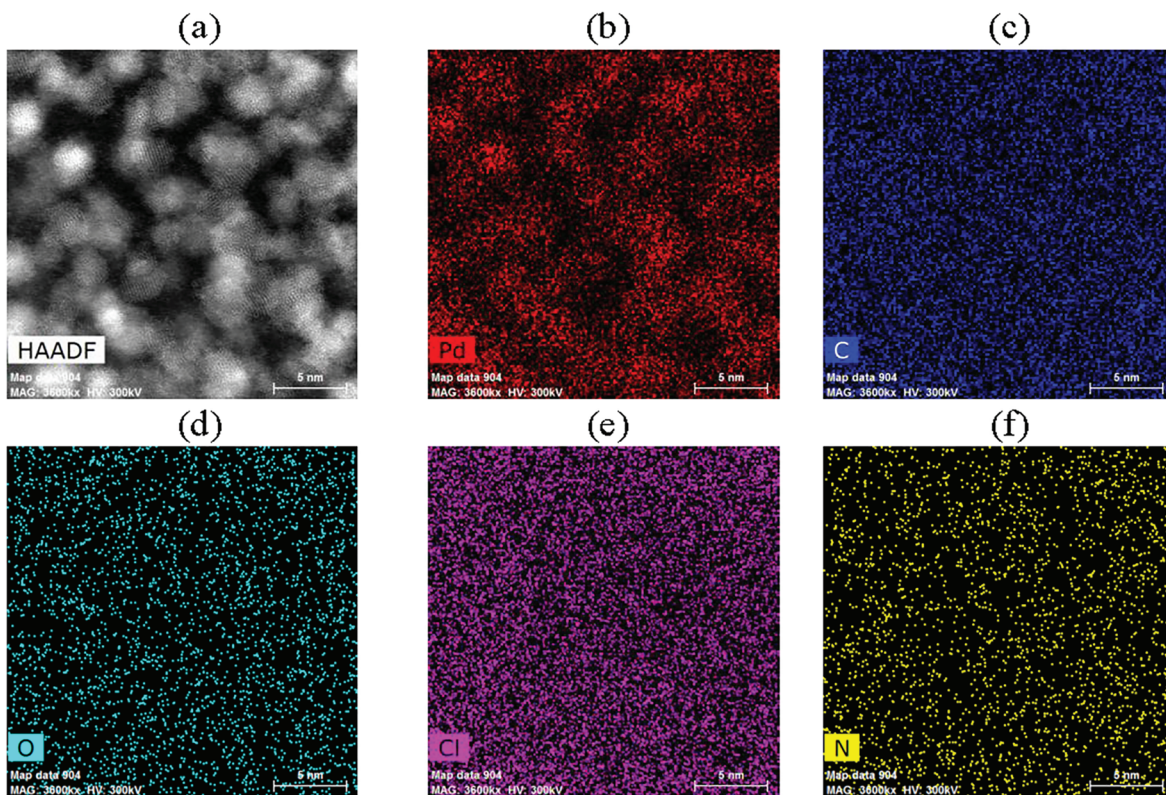


FIGURE 5 (a) HAADF-STEM image and (b)–(f) HAADF-STEM-EDX elemental mapping of Pd, C, O, Cl, and N elements in PdNPs/rGO-NH₂ nanocomposite

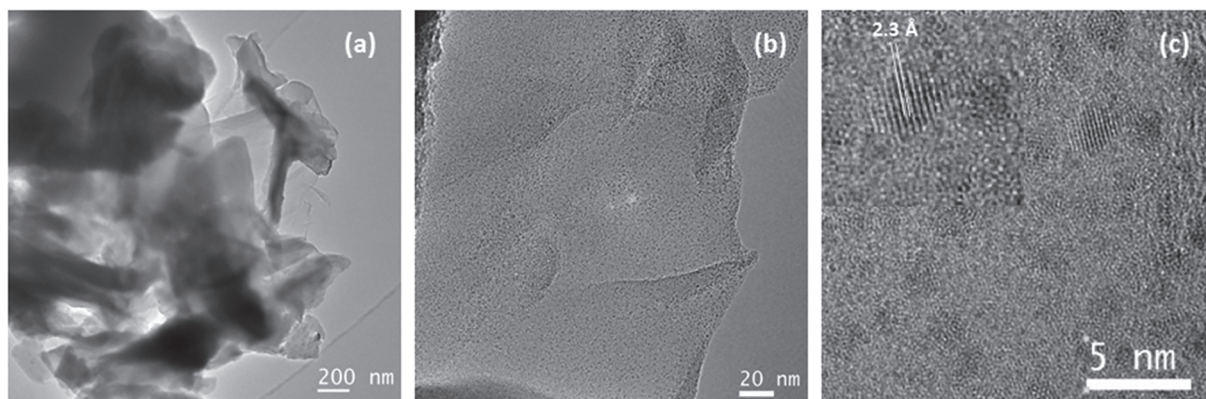
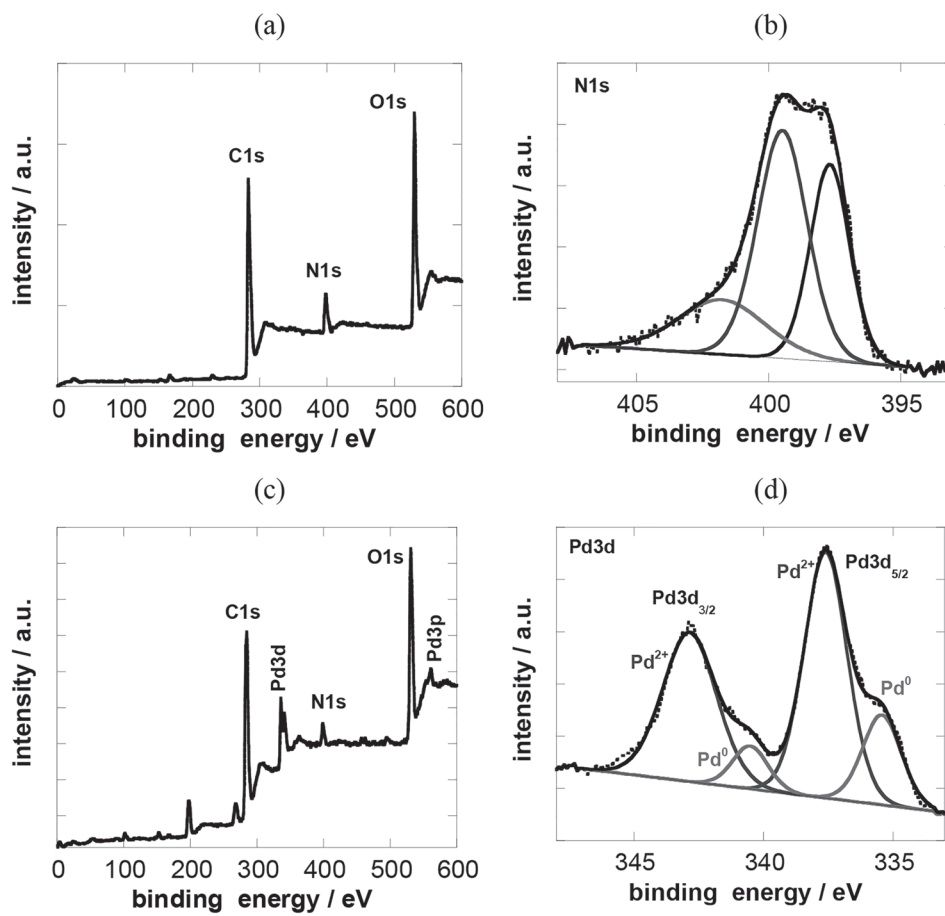


FIGURE 6 The TEM imaging of PdNPs/rGO-NH₂ nanocomposite. The inset corresponds to HRTEM of a single Pd nanoparticle

XPS wide-scan of rGO-NH₂ composite contains three peaks at ~285, 400, and 533 eV assigned to C_{1s}, N_{1s}, and O_{1s}, respectively (Figure 7a).^[25] The atomic composition of rGO-NH₂ composite consists of carbon (71.0 at%), oxygen (21.4 at%), and nitrogen (7.5 at%). As presented in Figure 7b, the XPS high resolution of the N_{1s} spectrum was deconvoluted into three peaks attributed to C–N (397.7 eV), N–H (399.8 eV), and NH₃⁺ (401.8 eV) bonds,^[25] with atomic percentages 32.50 at%, 47.61 at%,

and 19.98 at%, respectively. This result confirms the presence of N in this composite and is in complete agreement with EDX analysis. The XPS wide-scan spectrum of PdNPs/rGO-NH₂ nanocomposite contains six peaks at about 200, 285, 342, 400, 533 and 565 eV due to Cl_{2p}, C_{1s}, Pd_{3d}, N_{1s}, O_{1s}, and Pd_{3p}, respectively (Figure 7c),^[32] in agreement with EDX analysis. The atomic percentages are 69.12 at% (C), 24.33 at% (O), 4.45 at% (N), and 2.09 at% (Pd). The XPS high-resolution spectrum of the

FIGURE 7 (a) The XPS wide-scan and (b) the high-resolution spectrum of the N_{1s} of rGO-NH₂, (c) the XPS wide-scan and (d) the high-resolution spectrum of the Pd_{3d} of PdNPs/rGO-NH₂ nanocomposite

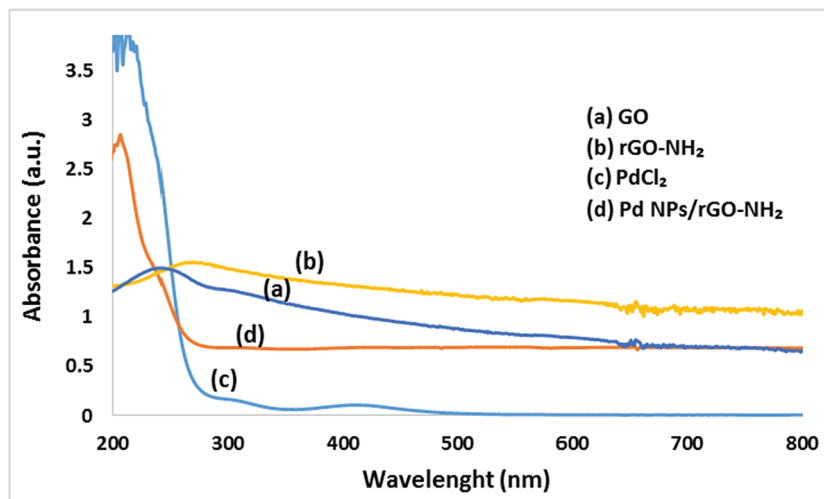


Pd_{3d} is deconvoluted into two components assigned to Pd²⁺ (337.3 and 342.9 eV) and Pd⁰ (335.4 and 340.4 eV)^[33] with a Pd²⁺/Pd⁰ ratio of 3.02, suggesting that palladium is dominantly in 2+ form along with a quantity of metallic Pd⁰ (Figure 7d). The XPS results established the presence of palladium in PdNPs/rGO-NH₂ nanocomposite, which is in total accordance with the EDX analysis. It should be noted that there have been several reports concerning the use of Pd²⁺^[12,34–37] or a

mixture of Pd²⁺/Pd⁰^[14,38] catalyst for the Mizoroki–Heck reaction.

The UV-visible (UV–Vis) absorption spectra of GO, rGO-NH₂, PdCl₂, and PdNPs/rGO-NH₂ are shown in Figure 8. The UV–Vis spectrum of GO dispersion in H₂O shows one major peak at ~230 nm and a weak peak at ~310 nm due to π–π* absorption of C=C bonds and n–π* absorption of C=O bonds, respectively^[39,40] (Figure 8a). The UV–Vis spectrum of rGO-NH₂ dispersion (Figure 8b)

FIGURE 8 UV–Vis spectra of (a) GO, (b) rGO-NH₂, (c) PdCl₂, and (d) PdNPs/rGO-NH₂ material



depicts a peak at ~260 nm, which confirms the chemical change in this material with respect to GO.^[29,30] The UV–Vis spectrum of PdCl₂ displays peaks at ~210, 240, 300, and 425 nm (Figure 8c).^[41] The UV–Vis spectrum of PdNPs/rGO-NH₂ nanocomposite comprises peaks at ~210 and 240 nm (Figure 8d). The disappearance of the peak at 425 nm as a result of the interaction of the surface of the substrate with the metal confirms the complexation of palladium by the substrate.^[42]

3.2 | Catalytic performance of PdNPs/rGO-NH₂ nanocomposite

In continuation of our investigation in catalysis,^[19–23,28,41] we assessed the efficacy of PdNPs/rGO-NH₂ nanocomposite as a heterogeneous catalyst for C–C bond formation via the Mizoroki–Heck cross-coupling reaction of aromatic halides with alkenes. The synthesis of methyl cinnamate from the reaction of iodobenzene (0.5 mmol) with methyl acrylate (1 mmol) in the presence of PdNPs/rGO-NH₂ nanocomposite (4 mg) was selected to optimize the coupling reaction. The results obtained for this reaction, under several conditions, are shown in Table 1. We first examined the influence of methanol, ethanol, acetonitrile, water, N-methyl-2-pyrrolidone (NMP), and DMF as solvent and 2 mmol of Et₃N, sodium hydroxide or potassium

carbonate as base for this coupling reaction (entries 1–7, Table 1). The results reveal that the C–C coupling reaction is dependent on the nature of the solvent; the yield of methyl cinnamate was higher when the reaction was conducted in DMF as a polar solvent and Et₃N at 120°C (entry 5, Table 1). Reducing the temperature to 100°C leads to a decrease of the yield of methyl cinnamate to 90% (entry 8, Table 1), indicating that 120°C is optimal for the Mizoroki–Heck coupling reaction under our experimental conditions. Decreasing the amount of PdNPs/rGO-NH₂ nanocomposite catalyst to 3 mg was accompanied by a decrease in the reaction yield to 80% (entry 7, Table 1), suggesting that 4 mg of PdNPs/rGO-NH₂ nanocomposite is required for this coupling reaction.

Using the optimized conditions, several aromatic iodo compounds (0.5 mmol), including iodobenzene, 4-iodotoluene, 4-idoanisole, 2-iodothiophene, and iodoferrocene, reacted with different alkenes (1 mmol) such as methyl, ethyl, and butyl acrylate, acrylic acid, and styrene in the presence of PdNPs/rGO-NH₂ nanocomposite (4 mg) in DMF (2 ml) and Et₃N (2 mmol) at 120°C to give the corresponding coupling compounds via the Mizoroki–Heck coupling reaction (Table 2).

The results reveal that the reaction of iodobenzene, 4-iodotoluene, 4-idoanisole, 2-iodothiophene, and iodoferrocene with methyl acrylate was successfully performed and the related coupling compounds were formed in high yields (69–100%) (entries 1–5, Table 2). It should be noted that the reaction of iodoferrocene with methyl acrylate takes place in high yield via the Mizoroki–Heck coupling reaction to produce new C–C bonds between the ferrocene group and methyl acrylate (entry 5, Table 2). We examined this coupling reaction for ethyl acrylate. The results indicate the high yield (95 and 83%) of coupling products for the reaction of 4-iodotoluene and iodoferrocene with ethyl acrylate, respectively (entries 6–7, Table 2). Next, we investigated the coupling reaction of butyl acrylate with aryl iodide using PdNPs/rGO-NH₂ nanocomposite. We observed the formation of C–C bonds via Mizoroki–Heck coupling of butyl acrylate with iodobenzene, 4-iodotoluene, and 4-idoanisole in 96%, 94%, and 98% yield, respectively (entries 8–10, Table 2). It should be noted that the reaction of iodoferrocene with butyl acrylate provided the corresponding coupling compound in trace even after a prolonged time of 17 hr at 120°C.

Similarly, the reaction of acrylic acid with iodobenzene and 4-iodotoluene produced cinnamic acid and 3-(*p*-tolyl)acrylic acid in 95% and 92% yield, respectively (entries 11–12, Table 2). Finally, we investigated the cross-coupling of styrene with iodobenzene and 4-idoanisole; the results revealed the synthesis of the

TABLE 1 Different conditions for the Mizoroki–Heck coupling reaction

Entry	Solvent	Base	Temperature (°C)	GC yield ^a (%)
1	MeOH	Et ₃ N	Reflux	38
2	EtOH	Et ₃ N	Reflux	61
3	CH ₃ CN	Et ₃ N	Reflux	90
4	NMP	Et ₃ N	120	97
5	DMF	Et ₃ N	120	100
6	DMF	NaOH	120	89
7	DMF	K ₂ CO ₃	120	81
8	DMF	Et ₃ N	100	90
9	DMF	Et ₃ N	120	80 ^b

DMF, dimethylformamide; GC, gas chromatography; NMP, *N*-methyl-2-pyrrolidone.

^aObtained by GC analysis with 1,4-dimethylbenzene as internal standard.

^bUsing 3 mg of catalyst.

TABLE 2 Mizoroki–Heck cross-coupling reaction of iodo and bromo compounds and different alkenes catalyzed by heterogeneous PdNPs/rGO-NH₂ nanocomposite

Entry	Ar	X	R	Product	GC yield ^{a,b} (%)
1	C ₆ H ₅	I	COOMe		100
2	4-Me-C ₆ H ₅	I	COOMe		95
3	4-OMe-C ₆ H ₅	I	COOMe		98
4	C ₄ SH ₃	I	COOMe		69
5	(C ₅ H ₅)Fe(C ₅ H ₄)	I	COOMe		91
6	4-Me-C ₆ H ₅	I	COOEt		95
7	(C ₅ H ₅)Fe(C ₅ H ₄)	I	COOEt		83
8 ^c	C ₆ H ₅	I	COOBu		96
9 ^c	4-Me-C ₆ H ₅	I	COOBu		94
10 ^c	4-OMe-C ₆ H ₅	I	COOBu		98
11 ^c	C ₆ H ₅	I	COOH		95
12 ^c	4-OMe-C ₆ H ₅	I	COOH		92
13 ^c	C ₆ H ₅	I	C ₆ H ₅		96 (15/1) ^d

(Continues)

TABLE 2 (Continued)

Entry	Ar	X	R	Product	GC yield ^{a,b} (%)
14 ^c	4-OMe-C ₆ H ₅	I	C ₆ H ₅		76 (12/1) ^d
15 ^e	C ₆ H ₅	Br	COOME		59
16 ^f	C ₆ H ₅	Br	COOBu		64

GC, gas chromatography.

^aReaction conditions: aromatic iodo compound (0.5 mmol), alkene (1 mmol), Et₃N (2 mmol), and 4 mg PdNPs/rGO-NH₂ catalyst in 2 ml of DMF at 120°C for 4 hr.

^bObtained by GC analysis with 1,4-dimethylbenzene as internal standard.

^c0.75 mmol of alkene was used.

^dThe number in parentheses corresponds to the ratio of *trans/cis* coupling compound.

^eThe reaction was performed with bromobenzene for 8 hr.

^fThe reaction was performed with bromobenzene for 10 hr.

related coupling compounds in 96% and 76% yield, respectively (entries 13–14, Table 2).

To broaden the scope of the reaction, we investigated the Mizoroki–Heck coupling reaction of methyl and butyl acrylate with bromobenzene under our optimized conditions. The results indicated that the coupling products, that is, methyl and butyl cinnamate, were formed in 59% and 64% yield after 8 and 10 hr, respectively (entries 15–16, Table 2). It should be noted that when the coupling reaction was performed with chlorobenzene under

otherwise identical conditions, the corresponding product was formed in trace after 24 hr. We conclude that our method is better suited for aromatic iodo compounds. This observation is in line with literature data indicating that the Mizoroki–Heck coupling reaction yield is high for iodo compounds.^[43–46]

The results obtained using PdNPs/rGO-NH₂ nanocomposite catalyst are comparable to those reported in the literature.^[12,34–36,47] For example, Basak and co-workers^[47] prepared methyl and butyl (*E*)-

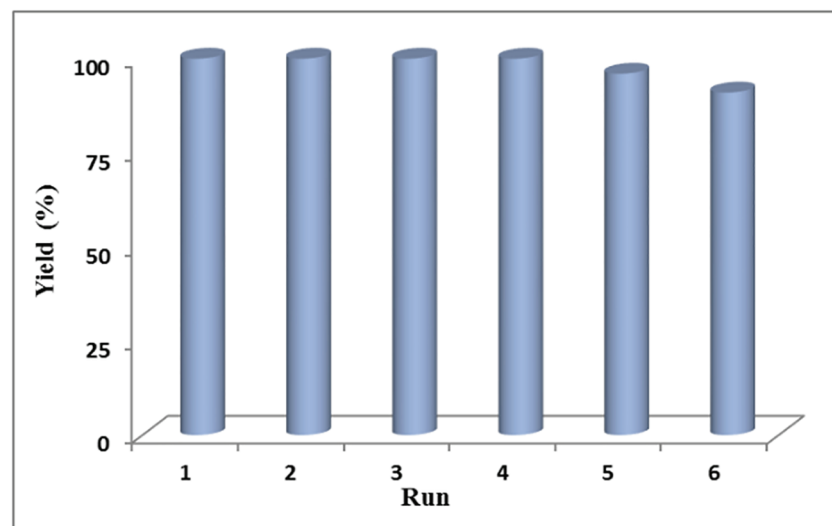


FIGURE 9 Recycling efficiency of heterogeneous PdNPs/rGO-NH₂ nanocomposite catalyst in a coupling reaction between iodobenzene with methyl acrylate at 120°C for 4 hr

3-(4-methoxyphenyl)acrylate in 85% yield by a coupling reaction of 4-iodoanisole with methyl or butyl acrylate using GO-poly(methyl methacrylate) supported palladium catalyst in the presence of tetrabutyl ammonium bromide as additive and K_2CO_3 as base at 100°C after 4 hr. The same products were synthesized using PdNPs/rGO-NH₂ nanocomposite catalyst in 98% yield (entries 3 and 10) in the presence of Et₃N after 4 hr at 120°C.

To estimate the reusability of the catalyst, the coupling reactions were executed several times with methyl acrylate and iodobenzene in DMF catalyzed by the recovered PdNPs/rGO-NH₂ (4 mg) nanocomposite catalyst. When the reaction was complete, the catalyst was recovered by centrifugation and washed with ethanol and dried in vacuum for reuse. The recovered heterogeneous catalyst was consecutively exposed to the a further five runs of the cross-coupling reaction using identical reaction conditions to the initial run. The results indicate that the recovered PdNPs/rGO-NH₂ catalyst is competent for the cross-coupling reaction of methyl acrylate and iodobenzene into methyl cinnamate in 91% yield even after six runs (Figure 9).

4 | CONCLUSION

A general and efficient procedure was established for the preparation of palladium nanoparticles loaded onto diethylenetriamine-functionalized rGO (PdNPs/rGO-NH₂) nanocomposite using an ultrasonic method. The structure and chemical composition of the PdNPs/rGO-NH₂ nanocomposite were fully characterized by several methods. The PdNPs/rGO-NH₂ material was successfully utilized as a heterogeneous catalyst for the coupling reaction of several aromatic iodo and bromo compounds with different alkenes via the Mizoroki-Heck reaction. Furthermore, the heterogeneous catalyst was reused for six successive runs without a significant diminution in its catalytic reactivity. This novel and simple procedure is valuable as the coupling reaction proceeds in great yields in short times.

ORCID

Maryam Mirza-Aghayan  <https://orcid.org/0000-0002-2214-5775>

REFERENCES

- [1] I. Favier, D. Madec, E. Teuma, M. Gomez, *Curr. Org. Chem.* **2011**, *15*, 3127.
- [2] A. Fihri, M. Bouhrara, B. Nekoueishahraki, J. -M. Basset, V. Polshettiwar, *Chem. Soc. Rev.* **2011**, *40*, 5181.
- [3] J. Hassan, M. Sevignon, C. Gozzi, E. Schulz, M. Lemaire, *Chem. Rev.* **2002**, *102*, 1359.
- [4] D. M. Huryn, Carbanions of Alkali and Alkaline Earth Cations:(ii) Selectivity of Carbonyl Addition Reaction, in *Comprehensive Organic Synthesis*, (Eds: B. M. Trost, I. Fleming), Pergamon Press, Oxford **1991**, Part, 1 49.
- [5] R. Mahrwald, D. Evans, *Modern aldol reactions*. Wiley Online Library, Wiley-VCH Verlag GmbH & Co. KGaA, Weinheim **2004**, Vol. 1 and 2, 1218.
- [6] B. D. Mather, K. Viswanathan, K. M. Miller, T. E. Long, *Prog. Polym. Sci.* **2006**, *31*, 487.
- [7] J. March, *Advanced organic chemistry: reactions, mechanisms, and structure*, John Wiley & Sons **1992**.
- [8] N. Miyaura, A. Suzuki, *Chem. Rev.* **1995**, *95*, 2457.
- [9] K. Sonogashira, *J. Organomet. Chem.* **2002**, *653*, 46.
- [10] R. F. Heck, J. Nolley Jr., *J. Org. Chem.* **1972**, *37*, 2320.
- [11] P. Das, W. Linert, *Coord. Chem. Rev.* **2016**, *311*, 1.
- [12] M. Keles, Z. Aydin, O. Serindag, *J. Organomet. Chem.* **2007**, *692*, 1951.
- [13] S. M. Sarkar, M. L. Rahman, M. M. Yusoff, *RSC Adv.* **2015**, *5*, 19630.
- [14] B. Urbán, D. Sránkó, G. Sáfrán, L. Úrge, F. Darvas, J. Bakos, R. Skoda-Földes, *J. Mol. Catal. A* **2014**, *395*, 364.
- [15] M. Gómez-Martínez, E. Buxaderas, I. M. Pastor, D. A. Alonso, *J. Mol. Catal. A* **2015**, *404*, 1.
- [16] Y. Lee, M. C. Hong, H. Ahn, J. Yu, H. Rhee, *J. Organomet. Chem.* **2014**, *769*, 80.
- [17] D. R. Dreyer, C. W. Bielawski, *Carbocatalysis: Chem. Sci.* **2011**, *2*, 1233.
- [18] M. Spiro, *Catal. Today* **1990**, *7*, 167.
- [19] M. Mirza-Aghayan, S. Zonoubi, M. M. Tavana, R. Boukherroub, *Ultrason. Sonochem.* **2015**, *22*, 359.
- [20] M. Mirza-Aghayan, M. M. Tavana, R. Boukherroub, *Tetrahedron Lett.* **2014**, *55*, 342.
- [21] M. Mirza-Aghayan, M. Alizadeh, M. M. Tavana, R. Boukherroub, *Tetrahedron Lett.* **2014**, *55*, 6694.
- [22] M. Mirza-Aghayan, M. M. Tavana, R. Boukherroub, *Tetrahedron Lett.* **2014**, *55*, 5471.
- [23] M. Mirza-Aghayan, M. M. Tavana, R. Boukherroub, *Cat. Commun.* **2015**, *69*, 97.
- [24] C. D. Zangmeister, *Chem. Mater.* **2010**, *22*, 5625.
- [25] A. Yang, J. Li, C. Zhang, W. Zhang, N. Ma, *Appl. Surf. Sci.* **2015**, *346*, 443.
- [26] M. Khan, G. H. Albalawi, M. R. Shaik, M. Khan, S. F. Adil, M. Kuniyil, H. Z. Alkhathlan, A. Al-Warthan, M. R. H. Siddiqui, *J. Saudi Chem. Soc.* **2017**, *21*, 450.
- [27] F. Chekin, *Bull. Mater. Sci.* **2015**, *38*, 887.
- [28] M. Mirza-Aghayan, E. Kashef-Azar, R. Boukherroub, *Tetrahedron Lett.* **2012**, *53*, 4962.
- [29] C. Vallés, J. D. Núñez, A. M. Benito, *Carbon* **2012**, *50*, 835.
- [30] J. Zhou, Y. Wang, X. Guo, J. Mao, S. Zhang, *Green Chem.* **2014**, *16*, 4669.
- [31] J. Yang, C. Tian, L. Wang, H. Fu, *J. Mater. Chem.* **2011**, *21*, 3384.
- [32] C. Bai, Q. Zhao, Y. Li, G. Zhang, F. Zhang, X. Fan, *Catal. Lett.* **2014**, *144*, 1617.
- [33] H. Huang, X. Wang, *J. Mater. Chem.* **2012**, *22*, 22533.
- [34] S. M. Sarkar, M. L. Rahman, K. F. Chong, M. M. Yusoff, *J. Catal.* **2017**, *350*, 103.

- [35] L. Fernández-García, M. Blanco, C. Blanco, P. Álvarez, M. Granda, R. Santamaría, R. Menéndez, *J. Mol. Catal. A* **2016**, *416*, 140.
- [36] M. S. Islam, M. L. Rahman, M. M. Yusoff, S. M. Sarkar, *J. Cleaner Prod.* **2017**, *149*, 1045.
- [37] M. Ghabdian, M. A. Nasseri, A. Allahresani, A. Motavallizadehkakhky, *Res. Chem. Intermed.* **2018**, *44*, 2929.
- [38] M. Kim, H. Kang, K. H. Park, *Cat. Com.* **2015**, *72*, 150.
- [39] T. Peng, H. Sun, T. Peng, B. Liu, X. Zhao, *Nanomaterials* **2017**, *7*, 292.
- [40] I. E. M. Carpio, J. D. Mangadlao, H. N. Nguyen, R. C. Advincula, D. F. Rodrigues, *Carbon* **2014**, *77*, 289.
- [41] M. Mirza-Aghayan, M. Kalantari, R. Boukherroub, *Appl. Organomet. Chem.* **2019**, *33*, e4837.
- [42] M. Adeli, E. Mehdipour, M. Bavadi, *J. Appl. Polym. Sci.* **2010**, *116*, 2188.
- [43] J. Zou, K. S. Iyer, S. G. Stewart, C. L. Raston, *New J. Chem.* **2011**, *35*, 854.
- [44] F. Durap, O. Metin, M. Aydemir, S. Oezkar, *Appl. Organomet. Chem.* **2009**, *23*, 498.
- [45] D. Liu, C. Zhang, F. Wang, Z. Huang, N. Zhang, H. Zhou, Y. Kuang, *J. Mater. Chem. A* **2015**, *3*, 16583.
- [46] V. Campisciano, V. La Parola, L. F. Liotta, F. Giacalone, M. Gruttadaria, *Chem-Eur J.* **2015**, *21*, 3327.
- [47] P. Basak, P. Ghosh, *Synth. Commun.* **2018**, 2584.

SUPPORTING INFORMATION

Additional supporting information may be found online in the Supporting Information section at the end of this article.

How to cite this article: Mirza-Aghayan M, Mohammadi M, Addad A, Boukherroub R. Pd nanoparticles supported on reduced graphene oxide as an effective and reusable heterogeneous catalyst for the Mizoroki–Heck coupling reaction. *Appl Organometal Chem.* 2020;e5524. <https://doi.org/10.1002/aoc.5524>